Original Article

Evaluation the Efficacy of Reduced Graphene-based Nanofibers by Laser Irradiation for Tissue Engineering Application

Tahere Parvizi Kashkooli [1], Mohsen Hatami [1], Seyedeh-Sara Hashemi [2*], Zahra Shahhossein [2]

1. Faculty of Physics, Shiraz university of Technology, Shiraz, Iran
2. Burn and Wound Healing Research Centre, Shiraz University of Medical Sciences, Shiraz, Iran

***Corresponding Author:**

Seyedeh-Sara Hashemi,

Burn and Wound Healing Research Centre, Shiraz University of Medical Sciences, Shiraz, Iran

Email: sara_hashemi@sums.ac.ir

Received: 11/6/2024
Accepted: 07/2/2025

ABSTRACT

Background: Graphene oxide (GO) and reduced graphene oxide (rGO) are graphene-based nanomaterials (GBNs) gained a lot of interest in biomedical tissue engineering due to their large specific surface area, unique structure, excellent photo-thermal effect, pH response, and broad-spectrum antibacterial properties. We aimed to modify the properties of graphene oxide/polycaprolactone (GO/ PCL) scaffold by laser irradiation.

Methods: The scaffold was fabricated by electrospinning method and then laser irradiation was applied to improve the scaffold's properties. The solution containing of PCL and graphene oxide was combined in an optimized ratio and then transferred to an electrospinning syringe. The temperature distribution affected by laser energy on a scaffold was predicted by heat equation. The Crank-Nicholson numerical method in two dimensions was used in this regard. The morphological properties were evaluated by SEM, XRD, and IDFIX. MTT assay was applied for biocompatibility evaluation.

Results: The 808 nm wavelength and 800 mW power was ideal laser irradiation. SEM results showed the appropriateness of fibres. MTT results showed a significantly higher cell viability in PCL/rGO group compared to PCL/GO and PCL scaffolds ($p \leq 0.001$).

Conclusion: The conversion of GO into rGO led to the better morphology and the reduction of cytotoxicity that gave the scaffold superior properties. Hence, it is justifiable to construct a composite scaffold, enhanced with rGO, to improve its conductivity, mechanical properties, and biocompatibility in the context of tissue engineering.

KEYWORDS
Laser; Scaffold; Graphene Oxide; Reduced Graphene Oxide; Tissue Engineering

Please cite this paper as:
Parvizi Kashkooli T, Hatami M, Hashemi SS, Shahhossein Z. Evaluation the Efficacy of Reduced Graphene-based Nanofibers by Laser Irradiation for Tissue Engineering Application. World J Plast Surg. 2025;14(1):21-32.
doi: 10.61186/wjps.14.2.21

INTRODUCTION

Recently, graphene-based nanomaterials (GBNs) have emerged as a promising option for biomedical applications. GBNs have demonstrated remarkable potential as scaffolds in tissue engineering and have been successfully used in several tissue engineering studies[1, 2]. These carbon nanostructures are analogs of extracellular matrix, such as collagen

[DOI: 10.61882/wjps.14.2.21]

fibres, owing to their comparable size [3]. They exist in many functionalized iterations, including graphene oxide (GO) and reduced graphene oxide (rGO). These new nanomaterials exhibit distinctive characteristics, including unique surface properties, enhanced biocompatibility, photothermal effects, pH responsiveness, and a wide range of antibacterial activity [4]. GO is derived from graphene.

This highly oxidized graphene monolayer contains several oxygen-containing active groups, including carboxyl (-COOH), hydroxyl (-OH), carbonyl (-C=O), and epoxy (-O-)[5]. Go has strong water solubility and stability, making it ideal for cell-surface attachment, proliferation, and differentiation [6, 7]. Furthermore, the presence of oxygen-containing functional groups in GO facilitates extensive chemical functionalization, rendering GO a suitable substrate for biomolecular control. This characteristic plays a pivotal role in several physiologically relevant GO uses [8]. Simultaneously, GO exhibits amphiphilic properties and can be employed as a surfactant. Furthermore, empirical evidence has demonstrated that GO composite hydrogels could undergo gelation in an acidic environment while exhibiting a gel-sol transition in alkaline settings [9]. The inclusion of oxygen-containing functional groups in graphene solutions enhances both its stability and chemical reactivity.

However, it is worth noting that the presence of these functional groups might lead to a higher density of defects. This could compromise graphene's conductivity, mechanical strength, and optical characteristics [10]. The process of reducing GO functional groups results in rGO. In comparison to GO, rGO restores conductivity and a photothermal effect. Additionally, rGO has a higher degree of hydrophobicity than GO[11] . Research demonstrated that rGO exhibits enhanced thermal stability due to its relatively lower oxygenation degree [12]. Moreover, it exhibits lower cytotoxicity than GO, even at elevated doses [13, 14]. Optimized processes involving strong reduction conditions (thermal, chemical, laser, electrochemical) are required for the production of rGO from GO. Despite the vast and efficient application of rGO to bioengineering applications, the use of harsh chemicals and unpleasant manufacturing procedures remains a significant problem. The suggested approach should combine ease of implementation, quick processing, cheap cost, and environmental friendliness. Thermal and laser reduction of GO are effective solutions in this regard because they generate more ordered graphene. They also allow simultaneous reduction and exfoliation via the abrupt expansion of CO or CO2 gases evolving into graphene sheets. This is done during GO's quick thermal heating [15, 16]. Polycaprolactone (PCL) is a synthetic polymer and highly hydrophobic semi-crystalline polyester with superior mechanical properties and long biodegradation times [17]. The various methods have been developed for the fabrication of high-performance PCL nanofiber scaffolds, such as co-electrospinning PCL with other biopolymers or nanofillers and post-electrospinning modifications[18]. The combination of biopolymers significantly improves the hydrophilicity and cellular responses of PCL scaffolds[19].

Electrospinning is a simple and convenient method for producing micro/microfibers with fiber diameters ranging from tens of nanometres to micrometres [20]. Electrospinning allows the production of porous nanofibrous membranes with specific features, including 3D morphology, a large surface area-to-volume ratio, and high porosity. The structure of an electrospun nanofiber membrane mimics the nanofibrous environment provided by extracellular matrix (ECM) components, which provides a natural base for cell adhesion, migration, and proliferation [21]. This study was primarily focused on harnessing the benefits of laser irradiation as a convenient and efficient approach to converting GO into rGO. Additionally, we aimed to develop an electrospun scaffold composed of rGO and PCL by as a promising substrate for tissue engineering applications.

MATERIALS AND METHODS

Nanofibers Preparation

Graphene oxide was selected as a nanomaterial, and PCL was used as a polymer to make the scaffold. According to our previous experiments, 20% of PCL was optimal for preparation without a willow-like structure (scaffold defect)[22]. The solution containing PCL and graphene oxide was combined in an optimized ratio of three to one and transferred to an electrospinning syringe. The device voltage was set at 20 kV, and the distance from the syringe to the collector was 12 cm. The scaffold production rate was 1 ml per hour. Then, Laser irradiation was applied to improve the scaffold's properties.

[DOI: 10.61882/wjps.14.2.21]

Ethics approval

The study was ethically approved by National Institute for Medical Research Development of Iran Ministry of Health, Treatment and Education (IR.SUMS.REC.1399.247).

Estimation of temperature distribution

By using the heat equation, we found the temperature distribution affected by laser energy on a scaffold. We employed the Crank-Nicholson numerical method in two dimensions, to solve the heat equation numerically. Based on laser radiation power and duration, this simulation clarified the local and temperature distribution on the scaffold. Using the results of the calculations, the temperature distribution on the scaffold can be predicted computationally to prevent the scaffold from burning. The effect of heat on the release of the target drug or the effect on scaffold ingredients are both important to improve the properties of scaffolds.
The heat equation for investigating the temperature distribution because of laser radiation on the scaffolds was:

$$\frac{2K}{r}\ \frac{\partial T}{\partial r} + K\frac{\partial^2 T}{\partial r^2} + q^0 = \rho C_p\ \frac{\partial T}{\partial t} \quad (1)$$

We rewrote the heat equation in the Cartesian coordinate system in two dimensions. The laser beam and scaffold were analysed in two dimensions:

$$K\frac{\partial^2 T}{\partial x^2} + K\frac{\partial^2 T}{\partial y^2} + q^0 = \rho C_p\ \frac{\partial T}{\partial t} \quad (2)$$

The first sentence of this equation represents the temperature distribution at the x-axis on the scaffolding surface. The second sentence shows the temperature distribution at the y-axis on the scaffolding surface, and the third sentence shows the heat of the laser source. The sum of these three factors illustrates the rate of heat distribution in the scaffold, according to the type of scaffold in a certain period of time.
Also, ρ is the symbol of the density of matter, C_p was heating capacity, K was the symbol of thermal conductivity of the scaffold, and T was the symbol of temperature distribution that depends on the time and coordinates of x and y, i.e., T = T (x, y, t) and q^0 was the heat of a laser spot.

Scanning Electron Microscopy (SEM)

Scanning electron microscope (SEM, TESCAN, Vega3 model, CzechRepublic) was used to identify the physical structure of fibres.

X-Ray Diffraction (XRD) and IDEX

We used the XRD test to prove the materials in the scaffold and to phase out the samples. However, some of the results that were specified in this test, such as reduction of oxygen groups and laser ablation, could not be clearly cited. Therefore, we were able to describe laser ablation in detail using the IDEX test.

ID Fix report

To determine the exact percentage of elements in the scaffold, IDFIX report was used.

Isolation, culture, and identification of Human Umbilical Cord Mesenchymal Stem Cells (HUC-MSCs)

An umbilical cord sample was obtained sterilely from the newborn (after obtaining volunteer mothers' consent for cesarean sections) at Shiraz Mother and Child Hospital. It was then transferred under sterile conditions to the culture room. Under sterile circumstances, stem cells were isolated from the Wharton's jelly region, as previously described [23, 24]. To evaluate osteogenic and adipogenic differentiation capabilities, 50,000 Wharton's Jelly-derived mesenchymal stem cells (WJ-MSCs) were seeded onto 6-well plates. At 80% confluence, the medium was replaced with osteogenic and adipogenic media. The medium alteration was performed once every 2 days. Following a period of 21 days, a 10% formalin solution was applied for 20 minutes to stabilize the WJ-MSCs. After rinsing with deionized water, the cells were stained with Alizarin Red dye (Sigma-Aldrich) and Oil Red-O (Sigma-Aldrich). Osteogenic differentiation was evaluated using Alizarin red staining. This facilitated the visualization of calcium mineralized deposits and had a reddish hue. The adipogenic induction process may be seen by Oil Red-O staining, which results in distinct red-colored droplets. Mesenchymal stem cells (MSCs) were validated using flow cytometry using fluorescent

[DOI: 10.61882/wjps.14.2.21]

antibodies specific to CD45, CD34, CD44, and CD105.

Cell viability assays

To evaluate the cytotoxicity of nanofibers, the nanofibers were submerged in a 96-well plate with a modification of Alpha-Minimum Essential Medium (α-MEM) and incubated for 24 hours at 37 °C in a moist environment with 5% CO2. The WJ-MSCs were introduced into the fibres at a density of 2 $\times 10^4$ cells per well, followed by incubation for 24 hours, 48 hours, and 72 hours. The cells were treated with a 0.05% MTT solution followed by incubation at 37°C for 3 hours. Subsequently, the MTT was extracted, and the optical density (OD) was assessed utilizing an automated plate reader, specifically an enzyme-linked immunosorbent assay (ELISA) system, at a wavelength of 590 nm after a 10-minute period of solubilization of the tetrazolium salt crystals. The tests were performed in triplicate.

Statistical analysis

All experiments were conducted in triplicate and findings were presented as mean ±standard error (SE) of means. SPSS software (Version 18, SPSS Inc., IBM, Chicago, IL, USA) and GraphPad Prism 6 (GraphPad Software, Inc., La Jolla, CA, USA) were used for statistical analysis. For comparisons, Two-way analysis of variance (ANOVA) and Tukey's post hoc test were used. A $P \leq 0.05$ was considered significant.

RESULTS

We used the parameters in Table 1 to simulate the heat equation (1). Since the scaffold consists of two compounds, PCL and GO, we used weight averages for properties such as ρ density of matter, Cp heat capacity, K thermal conductivity and r absorption coefficient. Our laser power was 400 mW and 800 mW, focusing on 0.008 cm^2 of scaffold.

Temperature Distribution Analysis

In the simulation, temperature was assessed in relation to time and scaffold surface coordinates. We presented the results of the simulation in Figures 1(a-f) for different times (2, 4 and 10 seconds). The results indicated a uniform and Gaussian temperature distribution. Figure 1(a, b) shows the temperature distribution after 2s. Figure 1(a) and 1(b) represents

Table 1: The Graphene Oxide (Go), polycaprolactone (PCL), and scaffold parameters

Parameters	Go	PCL	Scaffold
ρ	2100kg/m^3[16]	1120kg/m^3[21]	1.7231e+03
C_p	708j/kgK[17]	1815.79j/kg.K[21]	984.3787
K	3.91w/mK[18]	0.20w/mK[22]	2.9825
n	1. 96[19]	1.48[23]	$N_{effective}$= 1.8400

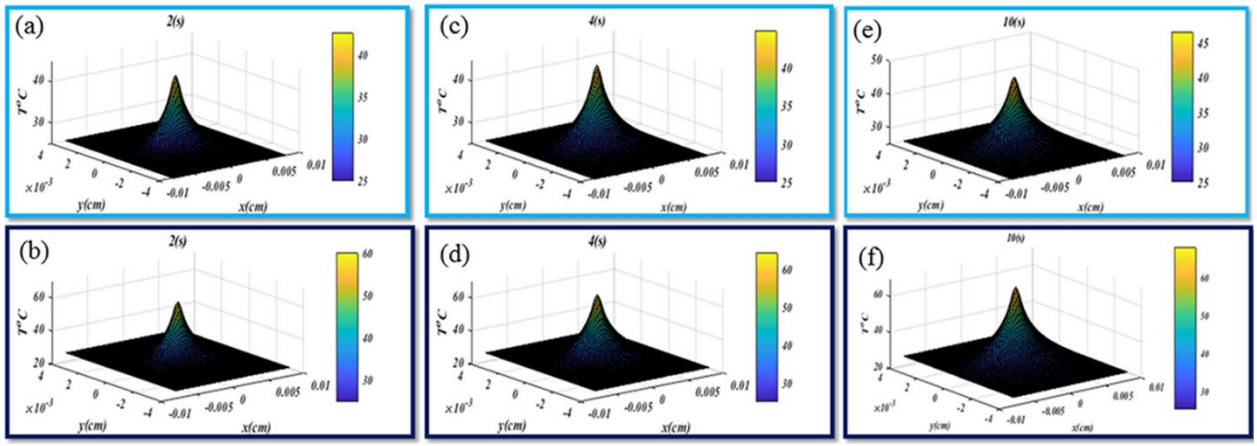

Figure 1: The result of simulating for temperature distribution in the scaffold at t = 2 seconds at 400mW (a) and at 800mW (b), t = 4 seconds at 400mW (c) and at 800Mw (d), and t = 10 seconds at 400mW (e) and at 800mW (f)

[DOI: 10.61882/wjps.14.2.21]

400mW and 800mW of laser irradiation, respectively. The maximum temperatures have reached 42 °C and 58 °C in Figure 1(a) and (b), respectively.

Also, in Figure 1(c, d), with the same parameters as in the previous figure, the temperature distributions showed at 4 seconds after laser light irradiation. According to Figure 1(c), the maximum temperature of a 400mW laser was 45°C, while the maximum temperature was 63°C for an 800mW laser. The temperature distribution in Figure 1 remains Gaussian.

In Figure 1(e, f), the results of simulations were displayed at 10s for input powers of 400 and 800mW in Figures 1(e) and 3(f), respectively. The maximum temperature almost reached to 47 °C and 68 °C in Figure 1(e, f). However, the temperature distribution was still uniform and Gaussian.

In Figure 2, scaffold temperature was calculated and plotted for 400 mW (a) and 800mW (b) during the period of time. Initially, the temperature increased

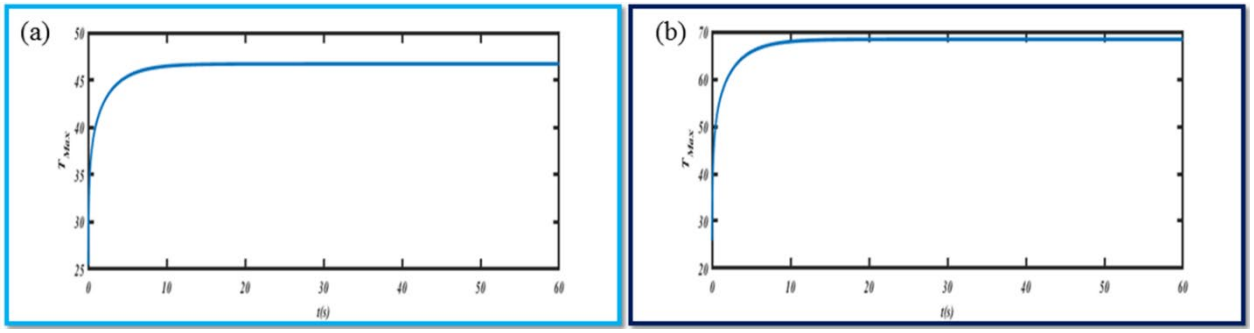

Figure 2: The maximum temperature reached by irradiation of laser on scaffold respected to time for 400mW (A) and at 800mW (B). In both of them nearly after 10 sec temperatures went to stable one, 46°C and 68 °C respectively

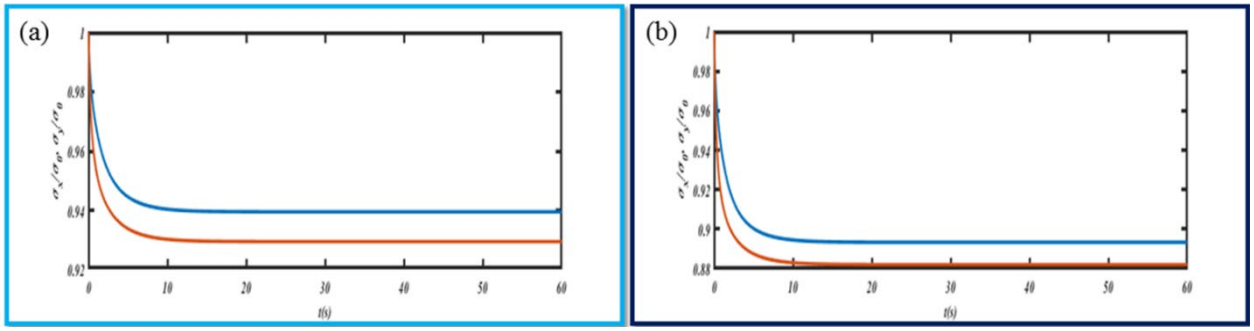

Figure 3: The result of simulating the heat distribution in a scaffold, which showed the ratio of the width of the temperature distribution of the laser beam σ(y)/σ(0) and σ(x)/σ(0) at wavelength of 808 nm and power of 400mW(a) and 800mW(b) in the x and y directions per unit time, relative to the original width

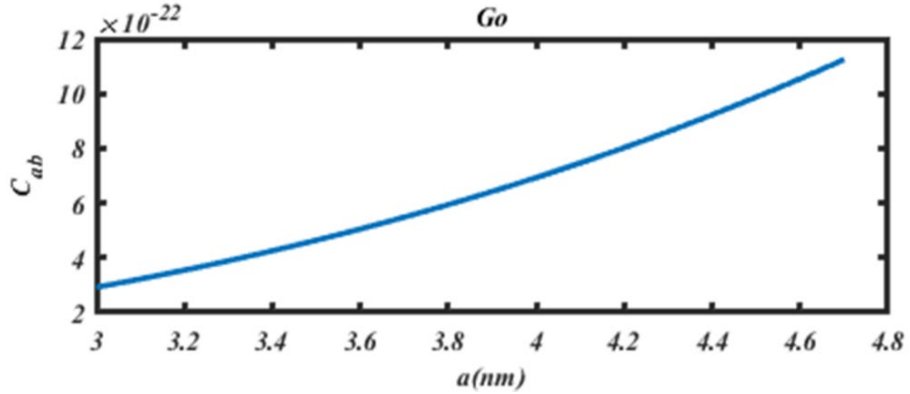

Figure 4: Laser absorption of Graphene Oxide

[DOI: 10.61882/wjps.14.2.21]

at a maximum rate after 10 seconds of irradiation, and then it reached a steady state. For 400 mW, the steady state value was 46 ℃ and for 800mW was 68 ℃.

The variation of normalized width of temperature distribution in the x and y direction during laser radiation was shown in Figure 3 for two laser power values. For 400 mW and 800 mW lasers, the width of thermal distribution decreased initially and then stabilized. We were able to determine how many times scaffolds needed laser irradiation using the results of the calculation.

According to the results of modelling the temperature distribution in the scaffold, assuming that we had a square scaffold with dimensions of 10 cm and a thickness of 1 mm, the diagrams showed that the temperature at the edges around the scaffold was constant at room temperature, but in the inside, the maximum temperature increased until about 68°C for about 10 seconds after laser beam (808 nm) at 800 mW power, and the maximum temperature reached to about 46 °C for about 10 seconds after laser beam (808 nm) at 400 mW power. As a result, the maximum temperature was reached and remained constant for 60 seconds.

Due to the fact that we considered the graphene oxide material with a size of 3-4.7 nm, we calculated the laser absorption rate of this material theoretically. In Figure 4, we have shown that with the increase in the size of the nanomaterial, the laser absorption was enhanced. This elevated the ablation effect of the laser.

In addition, we found that the effect of laser beams by 808 nm wavelength and 800 mW power was greater and more effective than laser beams by 808 nm wavelength and 400 mW power at the same time. The weight percentage and intensity of oxygen and carbon in both cases showed the appropriate effect of laser radiation on the scaffold, however, the laser beam with 800 mW power had more successful effects than 400 mW laser power.

Morphology of Scaffolds by SEM

To characterize the internal structures of the scaffold micrographs of fibres were captured by SEM (Figure 5). The appearance and the diameter of the fibres was measured in the magnification of 30,000. Images revealed that pores within the scaffolds are well distributed and highly interconnected, which is an essential characteristic for cell adhesion, migration and proliferation [25].

X-ray diffraction (XRD)

In Figure 6, we analysed the scaffold details with the XRD test. In this test, the existence of both components, such as GO and PCL had been shown

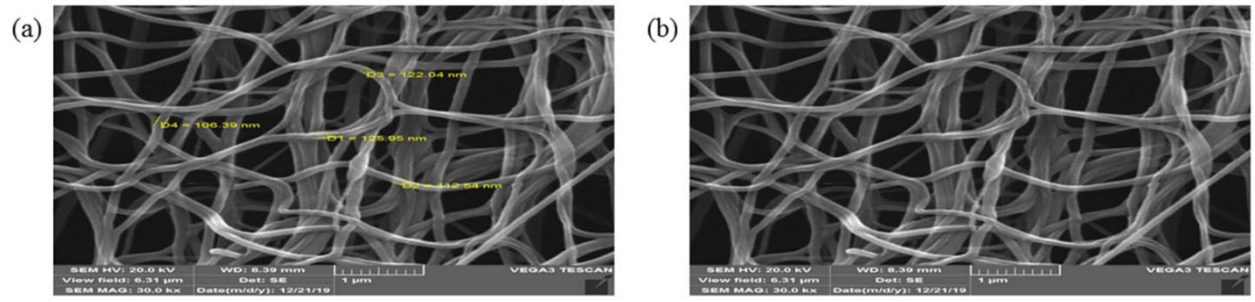

Figure 5: The size of the fibre's diameter made with a magnification of 30,000

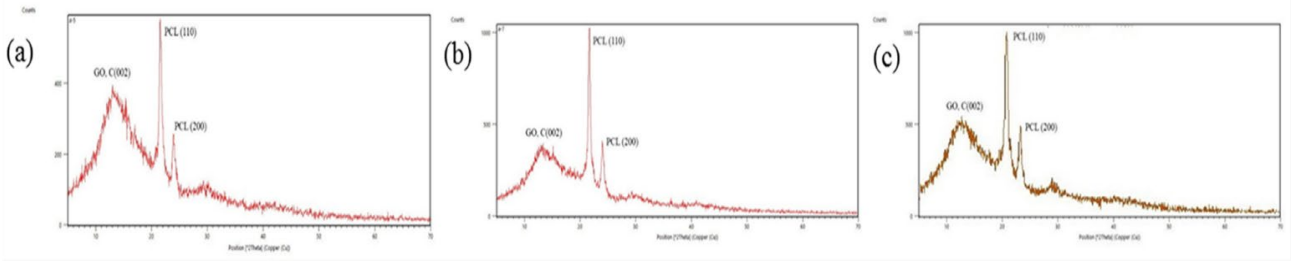

Figure 6: XRD analysis to determine the elements in the scaffold before (a) and after laser irradiation by 808 nm wavelength, 800 mW (b), and 400 mW (c) power for 8 minutes

[DOI: 10.61882/wjps.14.2.21]

well before and after laser irradiation.

ID Fix report

To determine the exact percentage of elements in the scaffolding, the IDFIX report was used (Figure 7). ID Fix test results depicted the percentage of carbon and oxygen elements before laser irradiation. Figure 7d, shows the weight presence of carbon and oxygen elements in the scaffold and the intensity (Int) before laser irradiation. The weight percentage of carbon was about 61.8% and its intensity was 719.2. Also, the weight percentage of oxygen was 38.05% and its intensity was 272.1. In Figure 7e Weight percentage of carbon in the scaffold after 808 nm laser radiation with a power of 800 mW shows 74.26%. The increase in carbon content was observed as its intensity reached to 870.5. The weight percentage of oxygen also increased from 38.05% to 25.74%, which was lower compared to the case without laser radiation, and this laser erosion had been a positive result of laser radiation to the scaffold. Oxygen intensity also decreased from 272.1 to 124.6 after laser irradiation.

According to Figure 7f, the weight percentage of carbon after radiation of 808 nm lasers with a power of 400 mW, has reached 70.67% compared to the state without laser irradiation. Carbon intensity has also reached 857.9. In addition, the weight percentage of oxygen after 808 laser irradiation with a power of 400 mW has increased from 38.05% in the sample without laser irradiation to 29.33%. In the presence of 808 lasers with a power of 400 mW, oxygen intensity has also reached 162. This implies a decrease in the amount of oxygen under the radiation of 808. Oxygen intensity has also reached 162, which under the radiation of 808 nm with a power of 400 mW, we see a decrease in the amount of oxygen.

Cell Characterization

WJ-MSCs were adherent to the culture plates and became spindle-shaped (Figure 8 a, b). Regarding osteogenic differentiation property, WJSCs illustrated calcium deposits in osteogenic media after three weeks that were visualized in red colour

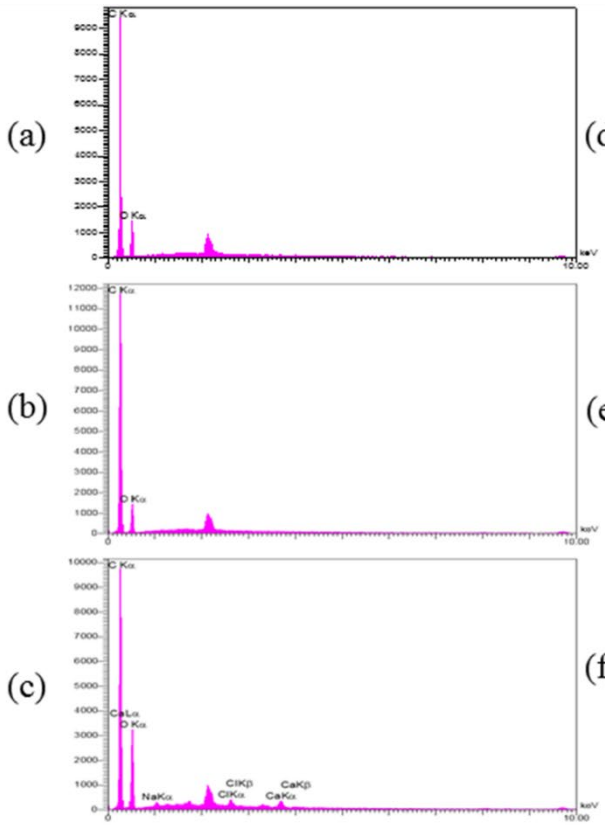

(d)

Elt	Int	W%
C	719.2	61.08
O	272.1	38.05

(e)

Elt	Int	W%
C	870.5	74.26
O	124.6	25.74

(f)

Elt	Int	W%
C	857.9	70.67
O	162.0	29.33

Figure 7: ID Fix test results. Graph showing the amount of carbon and oxygen elements before (a) and after laser irradiation by 808 nm wavelength, 800 mW (b) and 400 mW (c) power for 8 minutes. D, e and f indicates the percentage of carbon and oxygen elements in the scaffold and the intensity (Int) before (d) and after laser irradiation with a wavelength of 808 nm, a power of 800 mW (e) and 400 mW (f) for 8 minutes

[DOI: 10.61882/wjps.14.2.21]

by Alizarin Red staining (Figure8 c). In adipogenic induction, when WJSCs were stained by Oil Red-O revealed intracellular lipid droplets in red colour (Figure 8 d). These cells exhibited positive expression for CD44 and CD105 as mesenchymal markers and demonstrated negative expression for CD34 and CD45 as hematopoietic markers (Figure 8 e).

Cell viability

MTT assay was applied to analyse the cell viability and proliferation (Figure 9). The cell viability in PCL/rGO was significantly increased compared to PCL ($p \leq 0.01$, $p \leq 0.001$, respectively) and PCL/GO ($p \leq 0.05$) after 24h and 48 h. After 72 h, the PCL/rGO and PCL/GO groups significantly indicated higher cell viability than the PCL ($p \leq 0.001$, $p \leq 0.01$, respectively). Therefore, the conversion of GO into rGO led to the reduction of cytotoxicity.

DISCUSSION

Graphene, due to its exceptional properties, finds extensive applications in several fields, including energy, environmental science, healthcare, and sensor technology. GBNs have gained significant attention in the biomedical field, particularly in tissue engineering applications such as wound healing,

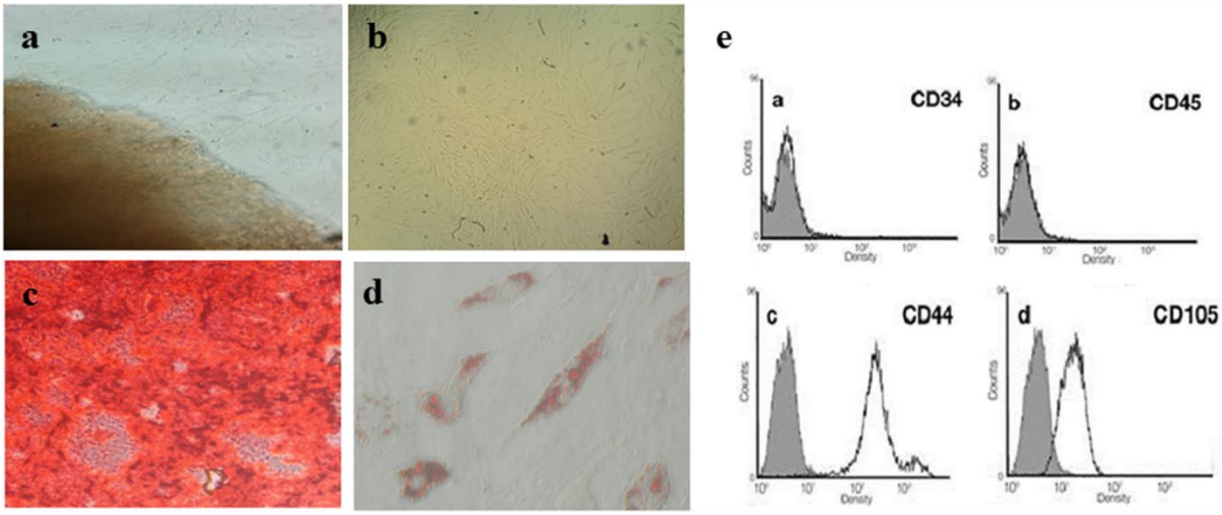

Figure 8: Characterization of hWJSCs: a: passage 1 (20x), b: passage 3 (20x), c: Osteogenic induction visualized in red color by Alizarin Red staining (40x), d: Adipogenic induction visualized in red color by Oil Red O staining (40x), e: Positive expression of mesenchymal stem cell markers for CD44 and CD105 and negative expression of hematopoietic stem cell markers for CD34 and CD45

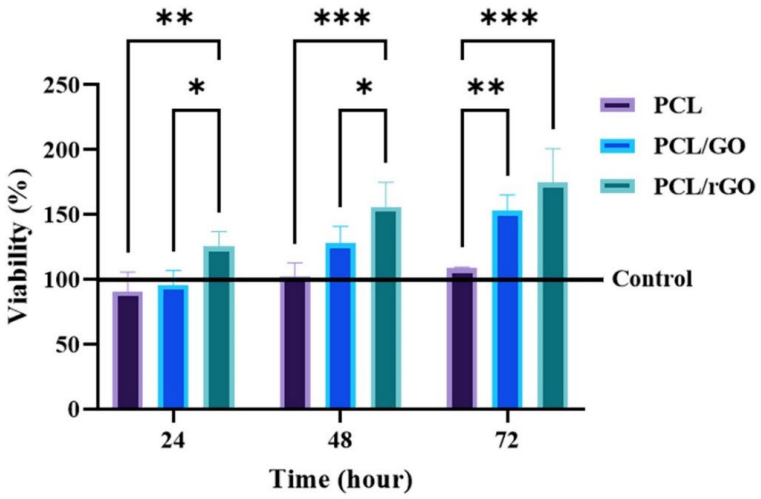

Figure 9: MTT assay comparing the viability in PCL, PCL/ GO and PCL/rGO nanofibers at 24, 48, and 72h after cell seeding. Data are expressed as mean ± SD. *p ≤ 0.05, **p ≤ 0.01 and ***p ≤ 0.001 compared to each other at the same time point

[DOI: 10.61882/wjps.14.2.21]

stem cell engineering, regenerative medicine, cell growth, and differentiation. This is primarily attributed to their exceptional mechanical strength and electrical conductivity. In addition, they have a diverse range of two-dimensional (2D) and three-dimensional (3D) structures [22, 26, 27]. Both GO and rGO nanoparticles promote stem cell proliferation and differentiation.

These nanoparticles can serve as scaffolds or components of scaffolds, rendering them very suitable for tissue engineering and regeneration applications, including skin[28-31] , cartilage [32], and bone [33-36]. RGO is frequently utilized as an additive in nanofibers to enhance their electrical conductivity. This attribute plays a crucial role in tissue regeneration, as evidenced by previous studies [37, 38]. This present work assessed the effectiveness of laser radiation in enhancing GO/PCL scaffold characteristics. The scaffold was generated using the electrospinning process, followed by the conversion of GO into reduced rGO using laser radiation. An optimal laser beam was identified through the use of a temperature distribution simulation. The laser beams selected for our purpose were those with a wavelength of 808 nm and a power of 800 mW since they were deemed the most suitable choice. Indeed, reduced rGO obtained from the reduction of GO under specific conditions exhibits distinct physicochemical characteristics that contribute to a decrease in cellular toxicity [39, 40].

Reduced rGO at a specific concentration level can stimulate angiogenesis. This effect is believed to be mediated by an increase in reactive oxygen species concentration inside the cells [41, 42]. Hence, it can be inferred that biomaterial scaffolds associated with reduced rGO provide advantages in terms of promoting cell adhesion and proliferation owing to their remarkable electroconductivity, lipophilicity, and biocompatibility, as shown by previous studies [43-45]. Hence, it is justifiable to construct a composite scaffold, enhanced with reduced rGO, to improve its conductivity, mechanical properties, and biocompatibility in the context of tissue engineering. Consistent with previous investigations, the utilization of laser erosion for the reduction of graphene oxide has been identified as a viable approach to enhance the efficacy of bio-scaffolds by enhancing their biocompatibility [46, 47]. Consistent with our findings, research conducted by Fu et al. examined the cytotoxic impact of the ADM/rGO and ADM-GO scaffolds at 24, 48, and 72 hours[48]. The prevalence of MSCs exhibited a progressive rise over time in all experimental groups. It is noteworthy that the cell viability on the ADM-GO exhibited a more pronounced reduction as the concentration increased, in contrast to the ADM-rGO[48]. The study demonstrated that the presence of a low concentration of ADM-rGO did not exhibit any cytotoxicity toward cells and instead, facilitated cell growth [48]. Therefore, the ADM-rGO scaffolds exhibited little cytotoxicity and demonstrated exceptional biocompatibility. Furthermore, a similar outcome was seen in another study done by Guo et al. [49]. A work conducted by Javier Cifuentes et al. involved the creation of innovative nanoengineered extracellular matrix scaffolds by the combination of small intestine submucosa (SIS) with GO and rGO. Consistent with our research findings, SEM pictures demonstrated that the scaffolds exhibit a uniform and extensive distribution of pores, which is a crucial attribute for facilitating cell adhesion, migration, and proliferation. However, contrary to our investigation, reduced rGO scaffolds resulted in a increase in cell survival. It was hypothesized that the observed inconsistency may be attributable to two distinct reduction procedures. Specifically, the chemical approach was employed in this investigation, whereas laser irradiation was used [50]. The reduction degree and characteristics of the resulting reduced rGO are significantly influenced by the kind of reduction agent [51].

Although GO and rGO exhibit favourable biocompatibility at lower concentrations, many pathways leading to cytotoxicity and genotoxicity have been found. These processes encompass cell membrane disruption and oxidative stress induced by these materials' aggregation. In future investigations, it is imperative to consider the cytotoxicity of GO and reduced rGO in relation to the ratio of nanoparticle size to cell size. In addition, it was shown that both GO and rGO exhibited a tendency to congregate within certain organs, even after functionalization. This situation is a matter of concern since although in vivo studies have typically classified these nanoparticles as non-lethal, certain toxic consequences have been observed. Due to the lack of research conducted on the long-term consequences, the application of GO/rGO as an in vivo nanocarrier in clinical studies is becoming increasingly challenging.

[DOI: 10.61882/wjps.14.2.21]

CONCLUSION

In this work, we successfully generated scaffolds composed of reduced graphene oxide and polycaprolactone using the electrospinning technique, followed by laser irradiation. The optimal laser beam was determined by the use of a temperature distribution simulation. The results indicated a high level of biocompatibility, as evidenced by the little cytotoxicity seen and the absence of any adverse effects on Wharton's jelly mesenchymal stem cells. Moreover, the pore size of the nanoengineered scaffolds further supports their potential for effective utilization in several domains, including regenerative medicine, tissue engineering, and wound healing. Future studies should prioritize the examination of other mechanical features of the scaffolds. In addition, they should explore their many uses and compatibility with key physiological conditions. Ultimately, it was of the utmost significance to thoroughly examine the impact of the constructed scaffolds on cellular proliferation and cytotoxicity in extended stimulation tests, as well as in diverse cell lines and even in vivo.

ACKNOWLEDGMENTS

This research received no fund. We would like to express their gratitude to the Burn and Wound Healing Research Centre at Shiraz University of Medical Sciences for the invaluable assistance.

CONFLICT OF INTEREST

The authors declare no conflict of interest.

REFERENCES

1. Karimi M, Mosaddad SA, Aghili SS, Dortaj H, Hashemi SS, Kiany F. Attachment and proliferation of human gingival fibroblasts seeded on barrier membranes using Wharton's jelly-derived stem cells conditioned medium: An in vitro study. *Journal of Biomedical Materials Research Part B: Applied Biomaterials* 2024;**112**(1):e35368.
2. Martinelli V, Bosi S, Peña B, et al. 3D Carbon-Nanotube-Based Composites for Cardiac Tissue Engineering. *ACS Appl Bio Mater* 2018 Nov 19;**1**(5):1530-7.
3. Minami K, Kasuya Y, Yamazaki T, et al. Highly Ordered 1D Fullerene Crystals for Concurrent Control of Macroscopic Cellular Orientation and Differentiation toward Large-Scale Tissue Engineering. *Adv Mater* 2015 Jul 15;**27**(27):4020-6.
4. Bonilla-Represa V, Abalos-Labruzzi C, Herrera-Martinez M, Guerrero-Pérez MO. Nanomaterials in Dentistry: State of the Art and Future Challenges. *Nanomaterials (Basel)* 2020 Sep 7;**10**(9).
5. Ding X, Liu H, Fan Y. Graphene-Based Materials in Regenerative Medicine. *Adv Healthc Mater* 2015 Jul 15;**4**(10):1451-68.
6. Bitounis D, Ali-Boucetta H, Hong BH, Min DH, Kostarelos K. Prospects and challenges of graphene in biomedical applications. *Adv Mater* 2013 Apr 24;**25**(16):2258-68.
7. Zhang K, Zheng H, Liang S, Gao C. Aligned PLLA nanofibrous scaffolds coated with graphene oxide for promoting neural cell growth. *Acta Biomater* 2016 Jun;**37**:131-42.
8. Nurunnabi M, Parvez K, Nafiujjaman M, et al. Bioapplication of graphene oxide derivatives: drug/gene delivery, imaging, polymeric modification, toxicology, therapeutics and challenges. *RSC Advances* 2015;**5**(52):42141-61.
9. González-Rodríguez L, Pérez-Davila S, Lama R, et al. 3D printing of PLA: CaP: GO scaffolds for bone tissue applications. *RSC Advances* 2023;**13**(23):15947-59.
10. Karlický F, Kumara Ramanatha Datta K, Otyepka M, Zbořil R. Halogenated Graphenes: Rapidly Growing Family of Graphene Derivatives. *ACS Nano* 2013 2013/08/27;**7**(8):6434-64.
11. Cabral CS, de Melo-Diogo D, Ferreira P, Moreira AF, Correia IJ. Reduced graphene oxide–reinforced tricalcium phosphate/gelatin/chitosan light-responsive scaffolds for application in bone regeneration. *Int J Biol Macromol* 2024;**259**:129210.
12. Konios D, Stylianakis MM, Stratakis E, Kymakis E. Dispersion behaviour of graphene oxide and reduced graphene oxide. *J Colloid Interface Sci* 2014;**430**:108-12.
13. Gurunathan S, Han JW, Kim JH. Green chemistry approach for the synthesis of biocompatible graphene. *Int J Nanomedicine* 2013;**8**:2719-32.
14. Muthoosamy K, Bai RG, Abubakar IB, et al. Exceedingly biocompatible and thin-layered reduced graphene oxide nanosheets using an eco-friendly mushroom extract strategy. *Int J Nanomedicine* 2015;**10**:1505-19.
15. Dolbin A, Vinnikov N, Esel'son V, et al. The effect of graphene oxide reduction temperature on the kinetics of low-temperature sorption of hydrogen. *Low Temp. Phys.* 2019;**45**(4):422-6.
16. Velasco A, Ryu YK, Boscá A, et al. Recent trends in graphene supercapacitors: from large area to microsupercapacitors. *Sustainable Energy Fuels*

[DOI: 10.61882/wjps.14.2.21]

2021;**5**(5):1235-54.
17. Alven S, Buyana B, Feketshane Z, Aderibigbe BA. Electrospun nanofibers/nanofibrous scaffolds loaded with silver nanoparticles as effective antibacterial wound dressing materials. *Pharmaceutics* 2021;**13**(7):964.
18. Ghosal K, Thomas S, Kalarikkal N, Gnanamani A. Collagen coated electrospun polycaprolactone (PCL) with titanium dioxide (TiO2) from an environmentally benign solvent: preliminary physico-chemical studies for skin substitute. *J Polymer Res* 2014;**21**(5):1-5.
19. Kumbar S, James R, Nukavarapu S, Laurencin C. Electrospun nanofiber scaffolds: engineering soft tissues. *Biomedical Materials* 2008;**3**(3):034002.
20. Xie X, Chen Y, Wang X, et al. Electrospinning nanofiber scaffolds for soft and hard tissue regeneration. *Journal of Materials Science & Technology* 2020;**59**:243-61.
21. Ma K, Chan CK, Liao S, Hwang WY, Feng Q, Ramakrishna S. Electrospun nanofiber scaffolds for rapid and rich capture of bone marrow-derived hematopoietic stem cells. *Biomaterials* 2008;**29**(13):2096-103.
22. Hashemi S-S, Mohammadi AA, Rajabi S-S, et al. Preparation and evaluation of a polycaprolactone/chitosan/propolis fibrous nanocomposite scaffold as a tissue engineering skin substitute. *BioImpacts: BI* 2023;**13**(4):275.
23. Hashemi S, Rafati A. Comparison between human cord blood serum and platelet-rich plasma supplementation for human wharton's jelly stem cells and dermal fibroblasts culture. *Int J Med Res Health Sci* 2016;**5**(8):191-6.
24. Hashemi SS, Mohammadi AA, Kabiri H, et al. The healing effect of Wharton's jelly stem cells seeded on biological scaffold in chronic skin ulcers: A randomized clinical trial. *J Cosmet Dermatol* 2019;**18**(6):1961-7.
25. Mitra T, Manna PJ, Raja STK, Gnanamani A, Kundu PP. Curcumin loaded nano graphene oxide reinforced fish scale collagen – a 3D scaffold biomaterial for wound healing applications. *RSC Adv* 2015;**5**(119):98653-65.
26. Li A, Zhang C, Zhang Y-F. Thermal Conductivity of Graphene-Polymer Composites: Mechanisms, Properties, and Applications. *Polymers* 2017;**9**(9):437.
27. Díez-Pascual AM, Luceño-Sánchez JA. Antibacterial Activity of Polymer Nanocomposites Incorporating Graphene and Its Derivatives: A State of Art. *Polymers* 2021;**13**(13):2105.
28. Asvar Z, Pirbonyeh N, Emami A, et al. Enhancing antibacterial activity against multi-drug resistant wound bacteria: Incorporating multiple nanoparticles into chitosan-based nanofibrous dressings for effective wound regeneration. *Journal of Drug Delivery Science and Technology* 2024;**95**:105542.
29. Amirsadeghi A, Jafari A, Hashemi S-S, et al. Sprayable antibacterial Persian gum-silver nanoparticle dressing for wound healing acceleration. *Materials Today Communications* 2021;**27**:102225.
30. Hashemi S-S, Pirmoradi M, Rafati A, Kian M, Mohammadi AA, Ali M. A human acellular dermal matrix coated with zinc oxide nanoparticles accelerates tendon repair in patients with hand flexor tendon injuries in zone 5 of the hand. *Bioimpacts* 2024;**14**(5):27748..
31. Sobhanian P, Khorram M, Hashemi S-S, Mohammadi A. Development of nanofibrous collagen-grafted poly (vinyl alcohol)/gelatin/alginate scaffolds as potential skin substitute. *Int J Biol Macromol* 2019;**130**:977-87.
32. Trucco D, Vannozzi L, Teblum E, et al. Graphene Oxide-Doped Gellan Gum–PEGDA Bilayered Hydrogel Mimicking the Mechanical and Lubrication Properties of Articular Cartilage. *Advanced Healthcare Materials 2021*;**10**(7):2001434.
33. Gohari PHM, Nazarpak MH, Solati-Hashjin MJMTC. The effect of adding reduced graphene oxide to electrospun polycaprolactone scaffolds on MG-63 cells activity. *Materials Today Communications* 2021;**27**:102287.
34. Jiao D, Zheng A, Liu Y, et al. Bidirectional differentiation of BMSCs induced by a biomimetic procallus based on a gelatin-reduced graphene oxide reinforced hydrogel for rapid bone regeneration. *Bioact Mater* 2021;**6**(7):2011-28.
35. de Lacerda Dantas PC, Martins-Júnior PA, Coutinho DCO, et al. Nanohybrid composed of graphene oxide functionalized with sodium hyaluronate accelerates bone healing in the tibia of rats. *Materials Science and Engineering: C* 2021;**123**:111961.
36. Aparicio-Collado JL, García-San-Martín N, Molina-Mateo J, et al. Electroactive calcium-alginate/polycaprolactone/reduced graphene oxide nanohybrid hydrogels for skeletal muscle tissue engineering. *Colloids Surf B Biointerfaces* 2022 Jun;**214**:112455.
37. Magaz A, Li X, Gough JE, Blaker JJ. Graphene oxide and electroactive reduced graphene oxide-based composite fibrous scaffolds for engineering excitable nerve tissue. *Mater Sci Eng C Mater Biol Appl* 2021 Feb;**119**:111632.
38. Zhang C, Wang X, Fan S, Lan P, Cao C, Zhang Y. Silk fibroin/reduced graphene oxide composite mats with enhanced mechanical properties and conductivity for tissue engineering. *Colloids and Surfaces B: Biointerfaces* 2021 2021/01/01/;**197**:111444.
39. Zhang Q, Liu X, Meng H, Liu S, Zhang C. Reduction pathway-dependent cytotoxicity of reduced graphene oxide. *Environmental Science: Nano* 2018;**5**(6):1361-71.

[DOI: 10.61882/wjps.14.2.21]

40. Tran T, Le HN, Tran V, Tran L, Vu T. Tithonia diversifolia pectin – reduced graphene oxide and its cytotoxic activity. *Materials Letters* 2016 07/01;**183**.
41. Mukherjee S, Sriram P, Barui AK, et al. Graphene Oxides Show Angiogenic Properties. *Adv Healthc Mater* 2015;**4**(11):1722-32.
42. Chakraborty S, Ponrasu T, Chandel S, Dixit M, Muthuvijayan VJRSOS. Reduced graphene oxide-loaded nanocomposite scaffolds for enhancing angiogenesis in tissue engineering applications. *R Soc Open Sci* 2018;**5**.
43. Kang Y, Liu J, Wu J, et al. Graphene oxide and reduced graphene oxide induced neural pheochromocytoma-derived PC12 cell lines apoptosis and cell cycle alterations via the ERK signaling pathways. *Int J Nanomedicine* 2017;**12**:5501-10.
44. Nie W, Peng C, Zhou X, et al. Three-dimensional porous scaffold by self-assembly of reduced graphene oxide and nano-hydroxyapatite composites for bone tissue engineering. *Carbon* 2017;**116**:325-37.
45. Syama S, Aby C, Maekawa T, Sakthikumar D, Mohanan PJDM. Nano-bio compatibility of PEGylated reduced graphene oxide on mesenchymal stem cells. *2D Materials* 2017;**4**(2):025066.
46. Savchenko A, Yin RT, Kireev D, Efimov IR, Molokanova E. Graphene-Based Scaffolds: Fundamentals and Applications for Cardiovascular Tissue Engineering. *Front Bioeng Biotechnol* 2021;**9**.
47. Bahrami S, Baheiraei N, Shahrezaee M. Biomimetic reduced graphene oxide coated collagen scaffold for in situ bone regeneration. *Sci Rep* 2021 2021/08/18;**11**(1):16783.
48. Fu J, Zhang Y, Chu J, et al. Reduced Graphene Oxide Incorporated Acellular Dermal Composite Scaffold Enables Efficient Local Delivery of Mesenchymal Stem Cells for Accelerating Diabetic Wound Healing. *ACS Biomaterials Science & Engineering* 2019 2019/08/12;**5**(8):4054-66.
49. Guo W, Wang S, Yu X, et al. Construction of a 3D rGO–collagen hybrid scaffold for enhancement of the neural differentiation of mesenchymal stem cells. *Nanoscale* 2016;**8**(4):1897-904.
50. Cifuentes J, Muñoz-Camargo C, Cruz JC. Reduced Graphene Oxide-Extracellular Matrix Scaffolds as a Multifunctional and Highly Biocompatible Nanocomposite for Wound Healing: Insights into Characterization and Electroconductive Potential. *Nanomaterials (Basel)* 2022 Aug 19;**12**(16).
51. Lesiak B, Trykowski G, Toth J, et al. Chemical and structural properties of reduced graphene oxide—dependence on the reducing agent. *J Materials Sci* 2021 02/01;**56**:1-17.

[DOI: 10.61882/wjps.14.2.21]